

# Tachyonic vs Quintessence dark energy: linear perturbations and CMB data

**Manvendra Pratap Rajvanshi<sup>1</sup>, Avinash Singh<sup>2</sup>, H.K. Jassal<sup>3</sup> & J.S. Bagla<sup>4</sup>**

Dept. of Physical Sciences, IISER Mohali, Sector 81, SAS Nagar, Punjab (India) - 140306

E-mail: <sup>1</sup>[manvendra@iisermohali.ac.in](mailto:manvendra@iisermohali.ac.in), <sup>2</sup>[avin.phy@gmail.com](mailto:avin.phy@gmail.com),  
<sup>3</sup>[hkjassal@iisermohali.ac.in](mailto:hkjassal@iisermohali.ac.in), <sup>4</sup>[jasjeet@iisermohali.ac.in](mailto:jasjeet@iisermohali.ac.in)

April 2021

**Abstract.** We use linear perturbation theory to study perturbations in dynamical dark energy models. We compare quintessence and tachyonic dark energy models with identical background evolution. We write the corresponding equations for different models in a form that makes it easier to see that the two models are very hard to distinguish in the linear regime, especially for models with  $(1 + w) \ll 1$ . We use Cosmic Microwave Background data and parametric representations for the two models to illustrate that they cannot be distinguished for the same background evolution with existing observations. Further, we constrain tachyonic models with the Planck data. We do this analysis for exponential and inverse square potentials and find that the intrinsic parameters of the potentials remain very weakly constrained. In particular, this is true in the regime allowed by low redshift observations.

## 1. Introduction

Observational evidence [1, 2, 3] of the accelerated expansion of the Universe spurred the search for theoretical models to explain the phenomenon. In these models, the candidate that drives this acceleration is an exotic, non-luminous, negative pressure medium, and it contributes approximately two-third of the energy budget of the Universe at present. This component called the dark energy (DE) [4, 5] can be one of several theoretical possibilities including modifications to the theory of gravity [6]. The standard model of cosmology ( $\Lambda$ CDM) represents dark energy by the cosmological constant: this is equivalent to an effective density and pressure that are constant in space-time. All other models are dynamical in nature. The existence of perturbations is a generic feature of dynamical dark energy models and hence offers a probing ground for theories. One of the most well-studied models of dark energy is quintessence [7, 8, 9, 10]: the minimally coupled scalar field. Another example is the tachyonic scalar field model [11, 12]. These and other dark energy models have a scale-dependent response to perturbations in the matter. Linear theory of cosmological perturbations [13, 14, 15] is used for studying

the evolution of fluctuations in dark energy. These can be used to compute transfer functions, cosmic microwave radiations anisotropies [16], and other observables.

Dark Energy perturbations have been studied in detail for quintessence [17, 18, 19, 20, 21]. Perturbation theory employs a split between background and perturbations over that background. Comparisons of dynamical dark energy models with standard  $\Lambda$ CDM show deviations in expansion history. Dark energy perturbations also induce differences in the power spectrum, CMB anisotropies, and other observables. For models allowing perturbations, the evolution is parameterized by a combination of background evolution (or expansion history) and characteristics of the model. This point needs careful consideration when comparing dark energy models. Their potentials often have tunable parameters that can be adjusted to get the same expansion history so that any observation based on background cosmology (e.g. supernova data) cannot be used to distinguish these. In that case, a question that can be asked is if perturbations-based observations show any difference between such models? We address this question from the perspective of linear theory. Further, we constrain tachyonic models with CMB data. Tachyonic models have been constrained with low redshift observations by Singh et. al [22, 23]. Here we use data from Planck 2018 data in addition to other observational datasets to constrain tachyonic models.

We present the results for quintessence and tachyonic models where we compare the growth of perturbations in linear theory. In the next two sections, we describe the formalism for writing perturbation equations that demonstrate explicitly that the difference between these two models diminish as we go towards  $w = -1$ . Specifically, it depends on factor  $(1 + w)$ , where  $w$  is the equation of state parameter. We demonstrate that differences between the two classes of models are suppressed by the factor  $(1 + w)$  and hence diminish rapidly as we approach closer to the cosmological constant. We also relate our formalism with earlier work as well as the fluid description. In section 4, we present the numerical results. In section 5, we use an approximate parametric representation for quintessence and tachyonic models to use CMB data to see if these can be distinguished by current data. We find that if the respective potentials for tachyonic and quintessence models are chosen such that the background evolution is identical then it is not possible to distinguish these with present observations. Finally, in section 6, we constrain two tachyonic models with CMB data. We summarize and comment on prospects in the last section.

## 2. Perturbation Theory

We consider scalar metric perturbations in the Newtonian gauge with the following form of the metric:

$$ds^2 = (1 + 2\psi)dt^2 - (1 - 2\xi)a^2(dx^2 + dy^2 + dz^2) \quad (1)$$

The problem of dark energy perturbations and its relevance for observables has been studied by many authors [24, 23, 25, 26, 17, 18, 19, 20, 21, 27]. Often, a fluid form

for dark energy is assumed. This fluid at the background level is characterized by the equation of state parameter ( $\bar{w}(z)$ ). For properly treating perturbations in fluid, one needs to know how energy density perturbations as well as pressure perturbations evolve. One can obtain dynamical equations for density perturbations and velocity perturbation either directly from Lagrangian density or from continuity equations (see Kodama & Sasaki [13], Bean & Dore [25] or Mukhanov [14], Ma & Bertschinger [15]). The set of equations derived in this manner is complete if additional information is provided for term  $\delta p/\delta\rho$ . In Newtonian gauge, ignoring anisotropic stress, we have [15]:

$$\dot{\delta} = -3H \left[ \left( \frac{\delta p}{\delta\rho} \right) - \bar{w} \right] \delta + 3(1 + \bar{w})\dot{\psi} - \frac{1 + \bar{w}}{a}\theta \quad (2)$$

$$\dot{\theta} = -(1 - 3\bar{w})H\theta - \frac{\dot{\bar{w}}}{1 + \bar{w}} + \frac{k^2\psi}{a} + \frac{k^2\delta}{(1 + \bar{w})a} \left( \frac{\delta p}{\delta\rho} \right) \quad (3)$$

where  $\delta$  is the fluid energy density contrast,  $\theta$  is defined as:

$$\theta\bar{\rho}(1 + \bar{w}) = -ik^j(\delta T)_j^0 \quad (4)$$

For adiabatic perturbations in fluids, there exists a relation between pressure perturbations and density perturbations. Using this relation we can eliminate pressure perturbations and solve for density perturbations. In general, one has to solve for both perturbations. In cases where density and pressure are effective quantities, e.g., scalar fields, the underlying system of equations has to be solved. A common approach is to quantify the variation of pressure perturbations using a gauge-invariant quantity called the effective speed of sound  $c_s^2$ . In an arbitrary gauge, pressure perturbations are written as [25, 28]:

$$(\delta p) = c_s^2(\delta\rho) + 3\dot{a}(1 + \bar{w})(c_s^2 - c_a^2)\bar{\rho}\frac{\theta}{k^2} \quad (5)$$

There are a few subtle points that need to be considered while using this definition:

- In order to ensure gauge invariance,  $c_s^2$  is defined in terms of  $\delta p/\delta\rho$  in a frame comoving with fluid, i.e., frame in which  $\theta$  is zero. Then from eq.(5),  $c_s^2$  is just  $\delta p/\delta\rho$  but in the frame comoving with fluid.
- In general, there are entropy perturbations as well. The gauge invariant amplitude of entropy perturbation is [13, 25]:

$$\bar{w}\Gamma = (c_s^2 - c_a^2)\delta \quad (6)$$

where  $c_a^2$  is a quantity determined by quantities related to evolution of the model background:

$$c_a^2 = \bar{w} - \frac{\dot{\bar{w}}}{3H(1 + \bar{w})} \quad (7)$$

For adiabatic perturbations,  $\Gamma$  vanishes, and  $c_a = c_s$ .

- Equation (5) can be derived [25] starting from eq.(6).  $\delta$  in general is not gauge invariant, but  $\delta$  in the frame comoving with the fluid is a gauge invariant quantity.  $\delta$  and  $\theta$  can be combined to form a gauge invariant quantity:

$$\delta_{rf} = \delta + 3\dot{a}(1 + \bar{w})\frac{\theta}{k^2} \quad (8)$$

In eq.(6), the left hand side is gauge invariant implying that combination on the right-hand side is gauge invariant too. Now we define  $c_s^2$  as  $\delta p/\delta\rho$  in the rest frame of fluid meaning each term on the right-hand side is individually gauge-invariant in the context of this definition. Then in any frame we can substitute for rest frame  $\delta$  using the quantity in eq.(8) in eq.(6) and then obtain eq.(5). For multicomponent systems, there can be an additional entropy perturbation besides intrinsic entropy perturbations [13]. This can be due to difference in dynamics (different  $c_a^2$ ) or due to non-minimal coupling. In such cases, working in terms of field variables is simpler and less prone to ambiguities.

- For scalar fields [29], let  $L(X, \phi)$  be the Lagrangian density, where  $X = \frac{1}{2}\partial_\mu\phi\partial^\mu\phi$  is the kinetic term while  $\phi$  is the field. Rest frame for field is defined as the one in which  $(\delta\phi)$  vanishes. In an arbitrary frame:

$$(\delta p) = \frac{\partial p}{\partial X}(\delta X) + \frac{\partial p}{\partial\phi}(\delta\phi) \quad (9)$$

with similar equation for  $(\delta\rho)$ . In rest frame:

$$(\delta p) = \frac{\partial p}{\partial X}(\delta X) \quad (10)$$

Combining equations for  $(\delta p)$  and  $(\delta\rho)$  in rest frame, we get

$$c_s^2 = \frac{(\delta p)}{(\delta\rho)} = \frac{p_{,X}}{\rho_{,X}} \quad (11)$$

where  $p_{,X}$  is partial derivative wrt  $X$ .

Earlier work [29, 25, 30, 27, 26, 24] along these lines has assumed some form for  $c_s^2$  and then constrained  $c_s^2$  and other parameters. These forms are assumed independent of  $\bar{w}(z)$ , thus the model is described by two functions. One general result from these studies is that the effects of different  $c_s^2$  but same  $\bar{w}(z)$  on observables are significant only in cases where dark energy has some significant contribution (at least a few percent) at time of recombination [29, 26]. But this itself means that  $\bar{w}(z)$  should be of such a form that dark energy has a significant contribution at early times. For scalar fields, given the form for Lagrangian density, there is no need of using any ad-hoc approximate form for  $c_s^2$ . Equations for systems with scalar field perturbations can be written entirely in terms of field perturbations (gauge-invariant) and perturbations in other constituents. But studies with effective parametrization of  $c_s^2$  are useful because they provide a general framework to compare different type of Lagrangian densities. Different Lagrangian densities may have different effective speeds of sound. For example, canonical scalar field Lagrangian of form:

$$L = X - V(\phi) \quad (12)$$

always have  $c_s^2 = 1$ , while k-essence ones with the form:

$$L = V(\phi)F(X) \quad (13)$$

can have a time-dependent  $c_s^2$ .

In this work, we consider the question whether two different scalar field Lagrangians (tachyonic and quintessence) with the same background evolution can be distinguished at the level of linear perturbations. Instead of working with an assumed form of  $c_s^2$  and using fluid equations, we directly work with scalar fields and their perturbations. Our model space is limited as we choose two specific Lagrangians, but our calculations are concrete with few assumptions. Our choice of formalism is well motivated by the question: all observations sensitive to background cosmology (only) give us a certain evolution of background quantities, then that can be explained by both quintessence and tachyonic models with corresponding reconstructed potentials. We explore if these models can be distinguished by observations sensitive to linear perturbations?

### 3. Basic equations for scalar fields with effective fluid approach

In this section, we derive equations for quintessence and tachyonic fields. For establishing correspondence between field description and the effective fluid description we define a new perturbation quantity:  $u$  which is the deviation in the equation of state from background homogeneous fluid. The fluid description we employ is slightly different from the standard approach but is useful in highlighting differences in quintessence and tachyonic models. We also give relations between standard fluid variables and the variables used here.

Let  $\Phi$  be the field for a scalar field representing dark energy. Then its stress energy tensor can be written as:

$$T_{\mu\nu} = (\rho + P)v_\mu v_\nu - P g_{\mu\nu} \quad (14)$$

where

$$v_\nu = \frac{\partial_\nu \Phi}{\sqrt{\partial^\alpha \Phi \partial_\alpha \Phi}} \quad (15)$$

We define first order quantities, density contrast and the corresponding variation in the equation of state parameter.

$$\rho = \bar{\rho}(1 + \delta) \quad W = \bar{w}(1 + u) \quad (16)$$

where variables with a bar are background quantities dependent on time only, while the first order variations ( $\delta$  &  $u$ ) can vary in space-time. We also define

$$\omega = 1 + \bar{w} \quad (17)$$

Effective pressure ( $P$ ) for a scalar field theory (with identification of  $P$  as per equation eq.(14)) is the Lagrangian ( $L_\Phi$ ) of field while the effective density  $\rho$  is:

$$\rho = 2g^{\mu\nu} \frac{\partial L_\Phi}{\partial g^{\mu\nu}} - L_\Phi \quad (18)$$

Writing the field as the sum of background and perturbation:

$$\Phi = \phi + (\delta\phi) \quad (19)$$

and substituting it in equation eq.(14), retaining only the first order terms, we get the first order stress energy tensor using metric eq.(1):

$$\begin{aligned} T_0^0 &= \bar{\rho}\delta \\ T_j^i &= \bar{\rho}(u + \delta)(1 - \omega) \quad \text{for } i = j \\ T_j^0 &= \frac{\bar{\rho}\omega}{\dot{\phi}} \frac{\partial(\delta\phi)}{\partial x^j} \end{aligned} \quad (20)$$

Off-diagonal spatial components of stress-energy tensor of both dark matter and field vanish at this order, hence the two metric potentials can be taken to be equal. We choose to work with  $\psi$ . The first order Einstein equation

$$G_1^1 = 8\pi G T_1^1 \quad (21)$$

can be used to obtain

$$\ddot{\psi} + 4\frac{\dot{a}}{a}\dot{\psi} + \psi \left[ \frac{2\ddot{a}}{a} + \frac{\dot{a}^2}{a^2} \right] = -4\pi G \bar{\rho}(u + \delta)(-\bar{w}) \quad (22)$$

We obtain the dynamical equations for  $\delta$  and  $u$  by requiring that the four divergence of stress energy tensor vanishes, i.e.

$$T_{\nu;\mu}^\mu = 0 \quad (23)$$

$$\dot{\delta} = 3u(1 - \omega)\frac{\dot{a}}{a} + \omega \left[ 3\dot{\psi} + \frac{\nabla^2(\delta\phi)}{a^2\dot{\phi}} \right] \quad (24)$$

Making use of the following off-diagonal Einstein equation:

$$\frac{\dot{a}}{a} \frac{\partial\psi}{\partial x^j} + \frac{\partial\dot{\psi}}{\partial x^j} = \frac{4\pi G \bar{\rho}\omega}{\dot{\phi}} \frac{\partial(\delta\phi)}{\partial x^j} + 4\pi G \frac{dm}{dm} T_j^0 \quad (25)$$

with dark matter stress energy contribution as

$$\frac{dm}{dm} T_j^0 = -a^2 \bar{\rho}_{dm} \frac{\partial U}{\partial x^j} \quad (26)$$

where  $U$  is dark matter velocity potential, we rewrite equation (24) as:

$$\dot{\delta} = 3u\frac{\dot{a}}{a}(1 - \omega) + 3\dot{\psi}\omega + \frac{1}{4\pi G \bar{\rho}a^2} \nabla^2 \left[ \frac{\dot{a}}{a}\psi + \dot{\psi} \right] + \frac{\bar{\rho}_{dm}}{\bar{\rho}} \nabla^2 U \quad (27)$$

We also get a constraint equation for  $u$

$$(-1 + \omega) \frac{\partial u}{\partial x^j} = (1 - \omega) \frac{\partial \delta}{\partial x^j} + \frac{\omega}{\dot{\phi}} \frac{\partial(\delta\phi)}{\partial x^j} \left[ 3\frac{\dot{a}}{a} + \frac{\dot{\bar{\rho}}}{\bar{\rho}} + \frac{\dot{\omega}}{\omega} \right] + \frac{\omega}{\dot{\phi}} \left[ -\frac{\ddot{\phi}}{\dot{\phi}} \frac{\partial(\delta\phi)}{\partial x^j} + \frac{\partial(\dot{\delta\phi})}{\partial x^j} \right] - \omega \frac{\partial \psi}{\partial x^j} \quad (28)$$

We observe that equations (22) and (27) do not have explicit dependence on particular details of scalar field (whether it is quintessence or tachyonic), but equation 28 does have such a dependence. Therefore any differences between models will arise from this equation. We rewrite these equations in a less “field-specific” form and find that the

equations in one of the theories have more terms. For tachyonic field, equation (28) can be written as:

$$\frac{(-1+\omega)}{2} \frac{\partial u}{\partial x^j} = (1-\omega) \frac{\partial \delta}{\partial x^j} + \left[ 3(1-\omega) \frac{\dot{a}}{a} + \frac{\dot{\omega}}{2\omega} \right] \left[ \frac{1}{4\pi G \bar{\rho}} \left( \frac{\dot{a}}{a} \frac{\partial \psi}{\partial x^j} + \frac{\partial \dot{\psi}}{\partial x^j} \right) + a^2 \frac{\bar{\rho}_{dm}}{\bar{\rho}} \frac{\partial U}{\partial x^j} \right] \quad (29)$$

While quintessence has extra terms in addition to those present in equation (29):

$$\frac{(-1+\omega)}{2} \frac{\partial u}{\partial x^j} = (1-\omega) \frac{\partial \delta}{\partial x^j} + \left[ 3(1-\omega) \frac{\dot{a}}{a} + \frac{\dot{\omega}}{2\omega} \right] \left[ \frac{1}{4\pi G \bar{\rho}} \left( \frac{\dot{a}}{a} \frac{\partial \psi}{\partial x^j} + \frac{\partial \dot{\psi}}{\partial x^j} \right) + a^2 \frac{\bar{\rho}_{dm}}{\bar{\rho}} \frac{\partial U}{\partial x^j} \right] + \omega \left[ \frac{3\dot{a}}{8\pi G \bar{\rho} a} \frac{\partial}{\partial x^j} \left( \frac{\dot{a}}{a} \psi + \dot{\psi} \right) + \frac{3\bar{\rho}_{dm} \dot{a} a}{2\bar{\rho}} \frac{\partial U}{\partial x^j} + \frac{1}{2} \frac{\partial \delta}{\partial x^j} \right] \quad (30)$$

Observing the third line in the above equation and comparing it with the equation for tachyonic counterpart (29), we find that the difference between two models is encoded in the terms multiplied by  $\omega = (1 + \bar{w})$ . For the models constrained by observations, this number is small, much smaller than unity. Effectively this makes the differences between two models a second order term.

We relate  $u$  to familiar quantities:

$$\frac{(u + \delta)\bar{w}}{\delta} = \frac{(\delta p)}{(\delta \rho)} \quad (31)$$

The effective “velocity” perturbation (coming from 4) for scalar field is:

$$\theta = \frac{k^2(\delta\phi)}{a\dot{\phi}} \quad (32)$$

and the effective speed of sound is:

$$c_s^2 = \frac{(u + \delta)\bar{w} + 3\frac{\dot{a}}{a}(1 + \bar{w})c_a^2 \frac{(\delta\phi)}{\dot{\phi}}}{\delta + 3\frac{\dot{a}}{a}(1 + \bar{w})\frac{(\delta\phi)}{\dot{\phi}}} \quad (33)$$

As stated earlier, we do not need to incorporate an effective  $c_s^2$  while working with fields because we have an analytical expression that can be evaluated. But for comparison of models, we derive approximate effective  $c_s^2$  for tachyonic field. Please note that  $c_s^2$  for quintessence is unity.

For tachyonic field the Lagrangian density is:

$$L(X, \Phi) = -V(\Phi) \sqrt{1 - 2X} \quad (34)$$

In the comoving frame of a scalar field:

$$c_s^2 = \frac{p_{,X}}{\rho_{,X}} = \frac{L_{,X}}{L_{,X} + 2L_{,XX}X} \quad (35)$$

In case of tachyonic field:

$$c_s^2 = (1 - 2X) = -\bar{w} - (1 + \bar{w})(\delta g^{00})_{rf} \approx -\bar{w} \quad (36)$$

In linear theory approximation  $c_s^2$  is just  $-\bar{w}$  as  $(1 + \bar{w}) \ll 1$  for models allowed by observations and the second term in eq.(36) is effectively of second order. Most of the comparisons of  $c_s^2$  in literature are between very different values of  $c_s^2$  like between 1, 0.1, 0.01, 0, etc. While we see that for models allowed by background observations, tachyonic  $c_s^2$  is not very different from quintessence value of 1.

In the following sections, we study the differences in the two models in linear theory using field perturbations. Note that one can either directly use equations derived from field perturbations or the fluid perturbations ( $u$  and  $\delta$ ) equations derived in this section as these are equivalent approaches.

#### 4. Results for field-based comparisons

We divide our discussion here into 2 subsections. In first we show comparisons for quantities, that influence observables, like metric potential ( $\psi$ ) and its derivative ( $\dot{\psi}$ ). In the second subsection, we show differences in dark energy perturbations.

##### 4.1. Influence on observables

All observables are affected by metric coefficients. The influence of these coefficients on dark matter linear growth rate is used in calculating observational effects like matter clustering,  $\sigma_8$ , growth index, etc. Rate of change of potential ( $\dot{\psi}$ ) affects CMB photons and causes observable effects like ISW [20, 31].

We present  $\psi$  and  $\dot{\psi}$  for the following background evolutions (characterized by  $\bar{w}(a)$ ):

- Constant  $\bar{w}(z)$  for values: - 0.5 and -0.975
- Chevallier-Polarski-Linder (CPL) parameterization [32, 33]

$$\bar{w} = w_0 + w_a \left(1 - \frac{a}{a_0}\right) \quad (37)$$

$\bar{w}(z)$  with parameters:  $w_0 = -0.9$  and  $w_a = -0.099$

Since differences in growth rate of perturbations with scale has been seen mainly at very large scales [17, 34, 35] we present results for length-scales: 2000 Mpc and 10000 Mpc. The differences between two models peak approximately around 10000 Mpc length-scales. At small scales, the growth of perturbations is suppressed, and at very large scales the growth rate is independent of the speed of sound. It is only in the transition region that we can expect to capture some differences between models with the same expansion history but a different  $c_s^2$ .

We show  $\psi$  and  $\dot{\psi}$  in figures 1,2 and 3. In the notation used to annotate the curves, we use ‘quin’ for quintessence models and ‘tach’ for the tachyon models. Also, we use red color for quintessence and black for the tachyonic field. The length scales are mentioned alongside. We find that tachyonic and quintessence models for  $\bar{w} = -0.975$  and CPL cases are almost indistinguishable with differences of the order 0.01% in most cases. Corresponding differences for  $\bar{w} = -0.5$  are more significant. These differences

grow in a monotonic and continuous manner as we moves away from  $w = -1$ . We plot one extreme case  $\bar{w} = -0.5$  that is observationally ruled out but gives an indication of the order of differences between the two classes of models. CPL and  $\bar{w} = -0.975$  are observationally allowed [36, 37] but differences between the models are extremely small at all scales. For  $w = -0.5$ , differences in potentials and its time derivatives can be of the order 10%.  $w = -0.975$  case shows negligible differences of the order 0.01% while CPL case has differences around 0.1%.

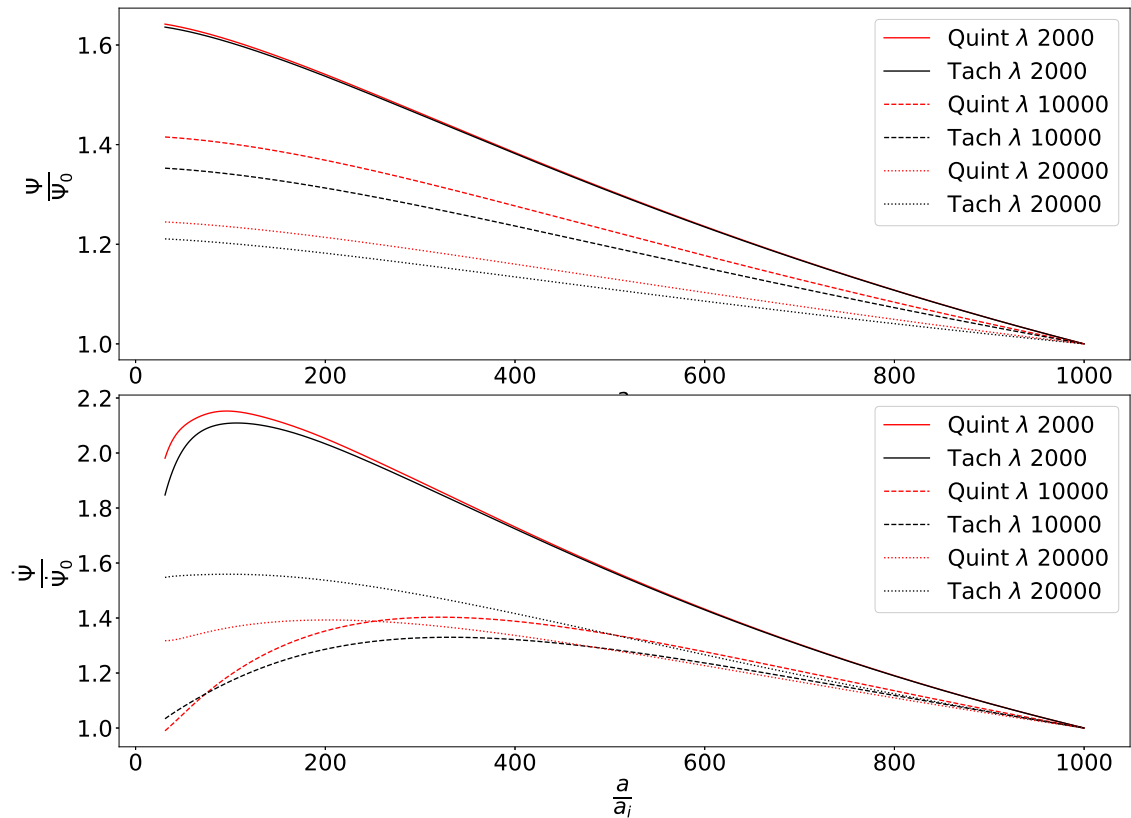


**Figure 1.** This figure shows the potential  $\psi$  and its time derivatives for  $\bar{w} = -0.5$ . The potentials have been normalized by their present day value. The difference in different models is higher for  $\lambda \sim 10k$ .

#### 4.2. Scalar fields

While dark energy perturbations show more differences (figures 4, 5 and 6) than potentials, their effects on observables are not very significant as shown in the previous subsection. Fluctuations are stronger for cases that are significantly removed from  $w = -1$ . Since dark energy perturbations are not directly observable, the significance

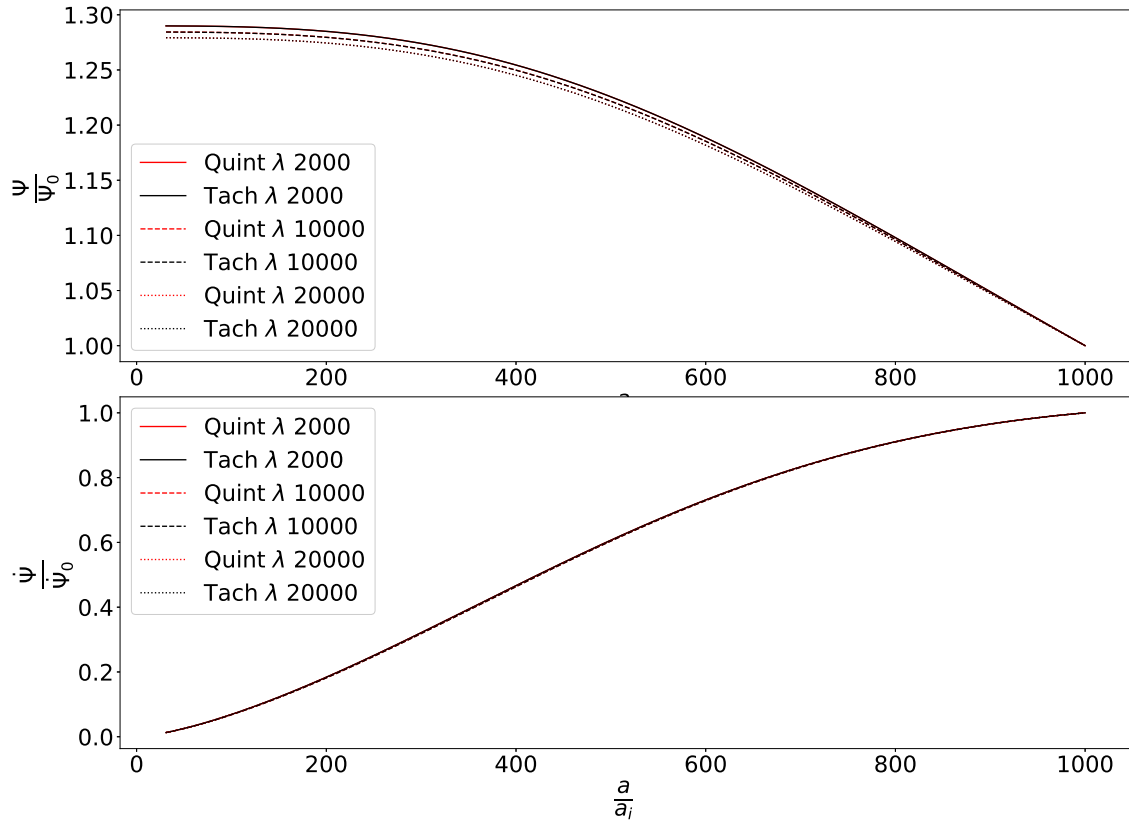


**Figure 2.** The plots show the potential  $\psi$  and its time derivatives for  $\bar{w} = -0.975$  case. Clearly, the relative differences are much smaller than in the case of  $w = -0.5$ .

of fluctuations can only be evaluated through observables as in the last subsection. We have shown comparisons for dark energy perturbations in figures 4, 5 and 6. Although there are visible differences (between tachyon and quintessence cases) in the evolution of DE perturbations but these differences remain insignificant because the amplitude of perturbations is very small.

## 5. Constraining models with CMB anisotropy data

There are two popular public codes available for CMB anisotropy calculations: CAMB [38] and CLASS [39, 40, 41]. Both have support for implementing fluid models with effective  $c_s^2$ . Here we use CLASS to calculate CMB anisotropy power spectra for effective  $c_s^2$  corresponding to tachyon models and quintessence models. This requires some minor tweaks in the default CLASS code as the standard version does not have time-dependent  $c_s^2$ . We modified the code to allow for a time-varying form of  $c_s^2$  for tachyon models. There are various ways tachyonic models can be included in CLASS. We can write

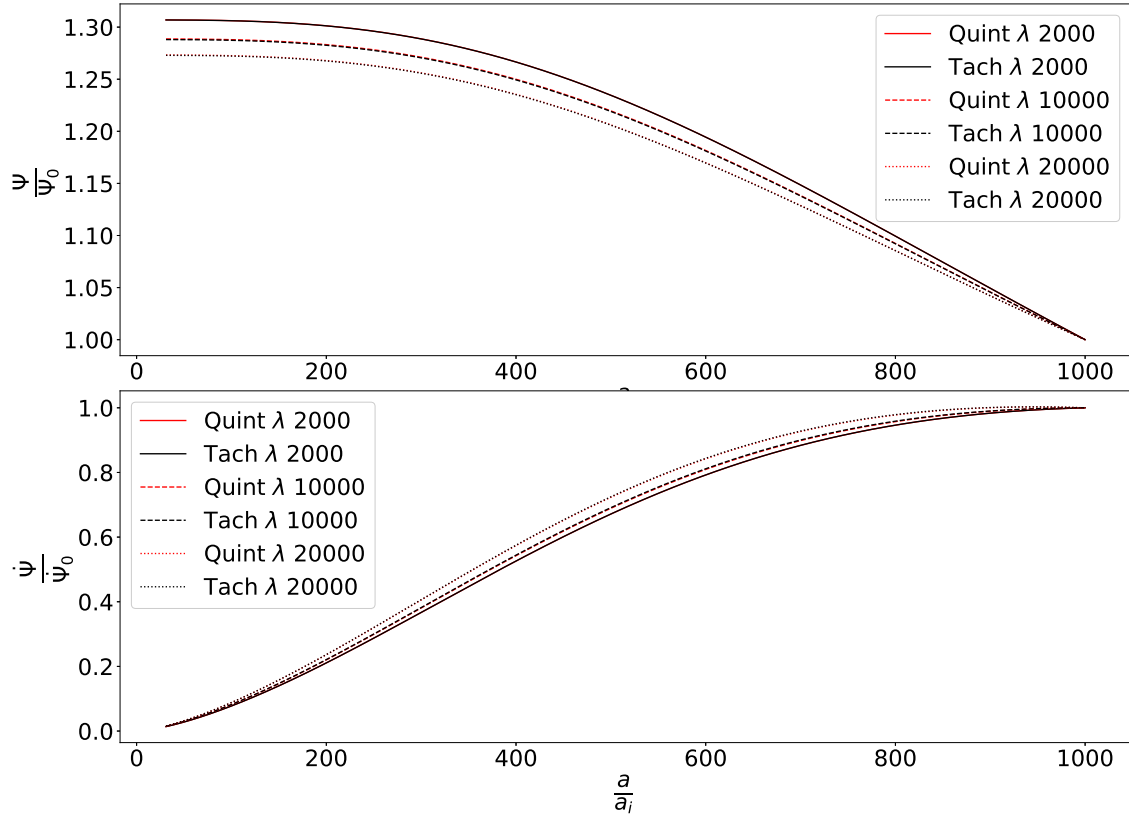


**Figure 3.** Here potential  $\psi$  and its time derivatives are plotted for the CPL model. Differences are much smaller than  $w = -0.5$  and slightly stronger than  $w = -0.975$  case. This is because in comparison to  $w = -0.975$ , the background evolution for the CPL model has a larger deviation from  $w = -1$ .

effective potentials for the tachyon field in terms of a chosen background DE (particular  $w(a)$ ), or we can have an effective fluid description with  $c_s^2$  as derived in eq.(36). While the former is a more apt and clean approach, the latter is easier to implement and is expected to give same results for  $(1 + \bar{w}) \ll 1$ , which anyway is the region already constrained by background cosmology probes. In cases where one has well-motivated forms for potentials, these tachyonic models can be implemented in CLASS with some more effort. We do this in the next section where we constrain tachyon models for two well-studied potentials.

We adopt following parametric form for  $c_s^2$ :

$$c_s^2 = c1 * w + c0 \quad (38)$$

This is the simplest form that can capture both quintessence and tachyonic models. For quintessence, we have  $c1 = 0$  and  $c0 = 1$  and for tachyonic models  $c1 = -1$  and  $c0 = 0$ . We then do an MCMC sampling using CLASS with MontePython [42, 43]. We

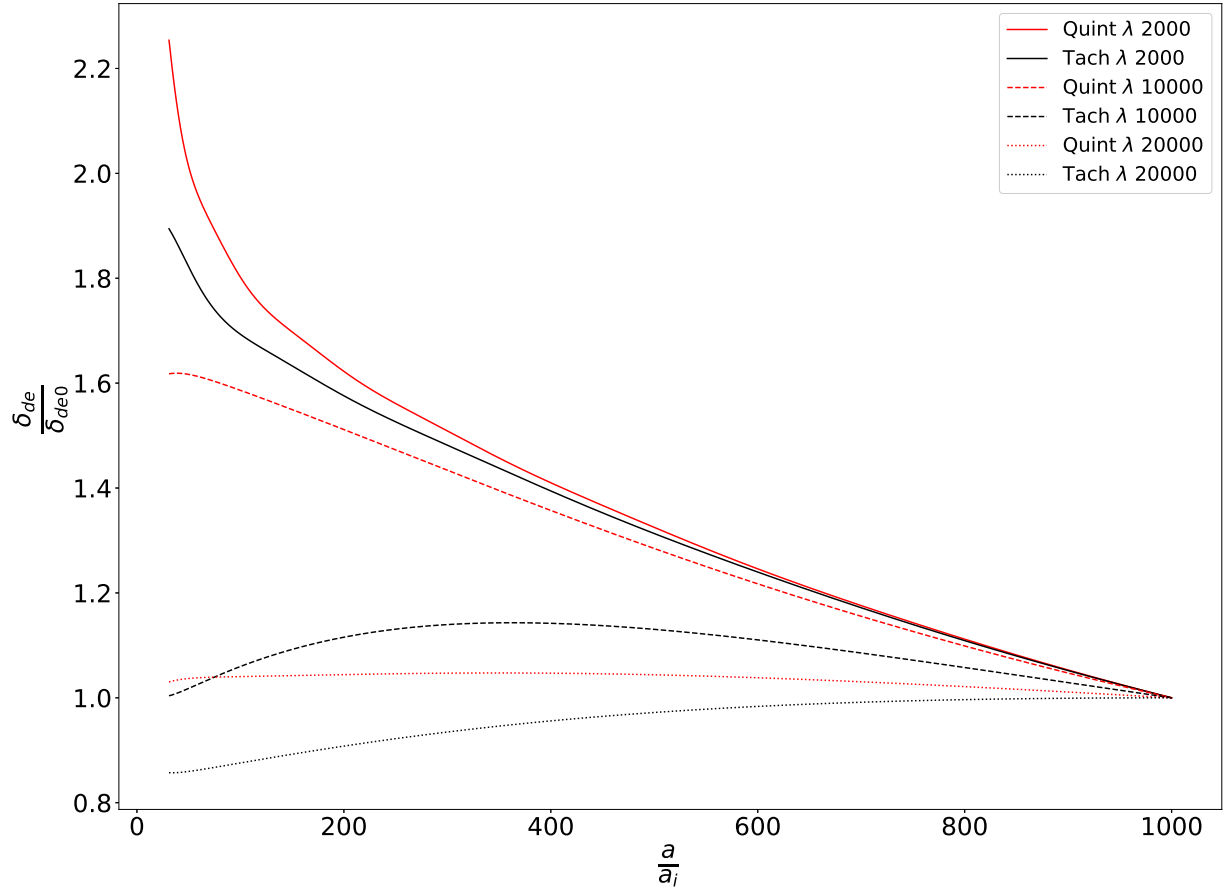


**Figure 4.** Dark energy (DE) density contrast for  $\bar{w} = -0.5$  case. It shows growth of DE normalized by present value.

use CMB (Planck 2018 high-l TT,TE,EE, low-l EE, low-l TT, lensing) [44] and BAO data (Boss Data Release 12 [45, 46], small-z BAO data from 6dF Galaxy Survey [47] and SDSS DR7 main Galaxy sample [48]). We find that the two parameters  $c1$  and  $c0$  remain unconstrained. In fig 7, we show triangle plots for 2d marginalized credible intervals. Parameters relating to DE speed of sound are unconstrained. This result is similar to analyses with constant  $c_s^2$  have obtained earlier [26, 24, 27, 25]. While the previous work deals with either constant  $c_s^2$  or some particularly chosen form, here we have chosen an explicit parameterized form for it, which encapsulates both quintessence and tachyonic field. In figure 8, we plot the marginalised posteriors.

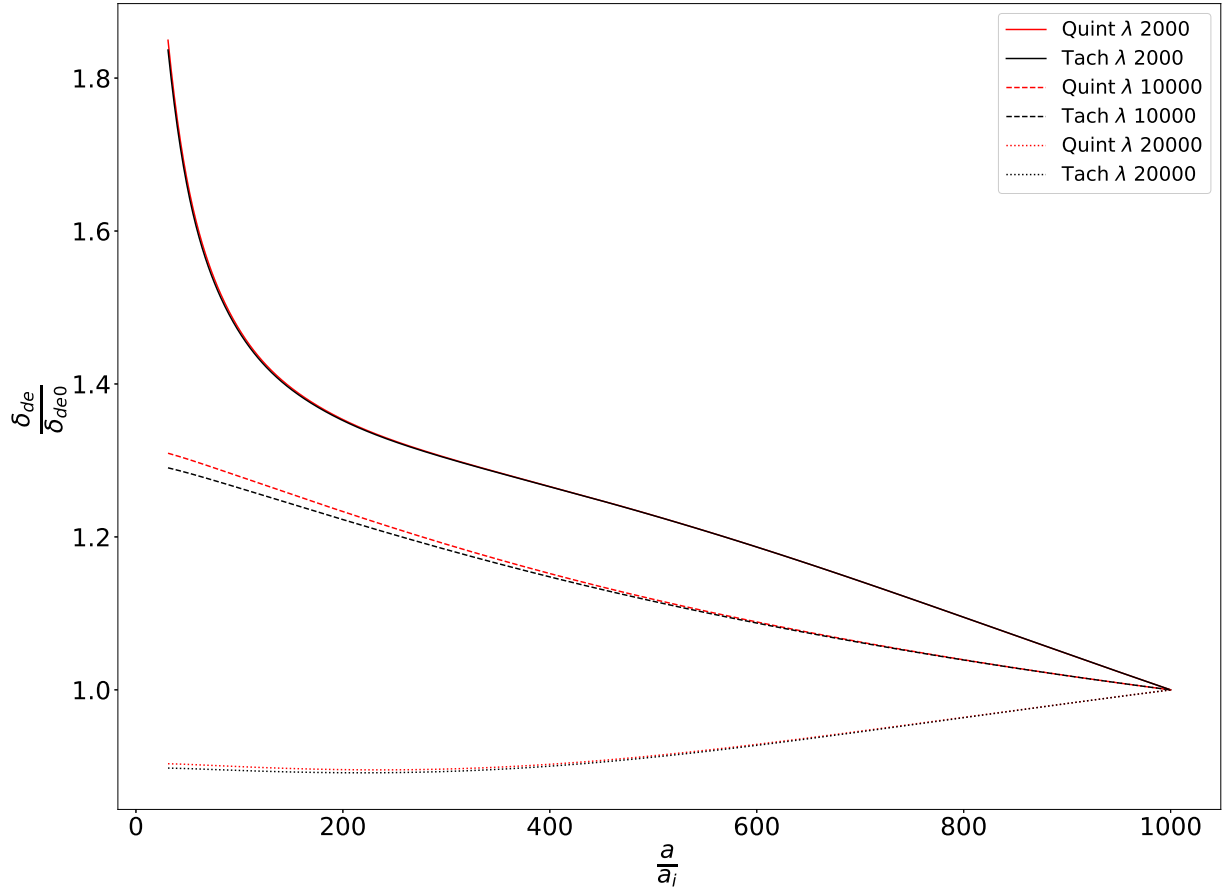


**Figure 5.** Dark energy (DE) density contrast for  $\bar{w} = -0.975$  case. Relative differences between quintessence and tachyonic models are small in comparison with  $w = -0.5$  case.

## 6. CMB data and tachyonic models

We modify CLASS to implement tachyonic models as a scalar field at linear level, where equations are obtained from Lagrangian corresponding to tachyonic dark energy (The equations and modifications related information is provided in Appendix A). Two potentials which we code in CLASS are:

- Exponential potential

$$V(\phi) = V_0 \exp\left(-\frac{\phi}{\phi_a}\right) \quad (39)$$

- Inverse Square Potential

$$V(\phi) = \frac{n}{4\pi G} \left(1 - \frac{2}{3n}\right)^{\frac{1}{2}} \frac{1}{\phi^2} \quad (40)$$

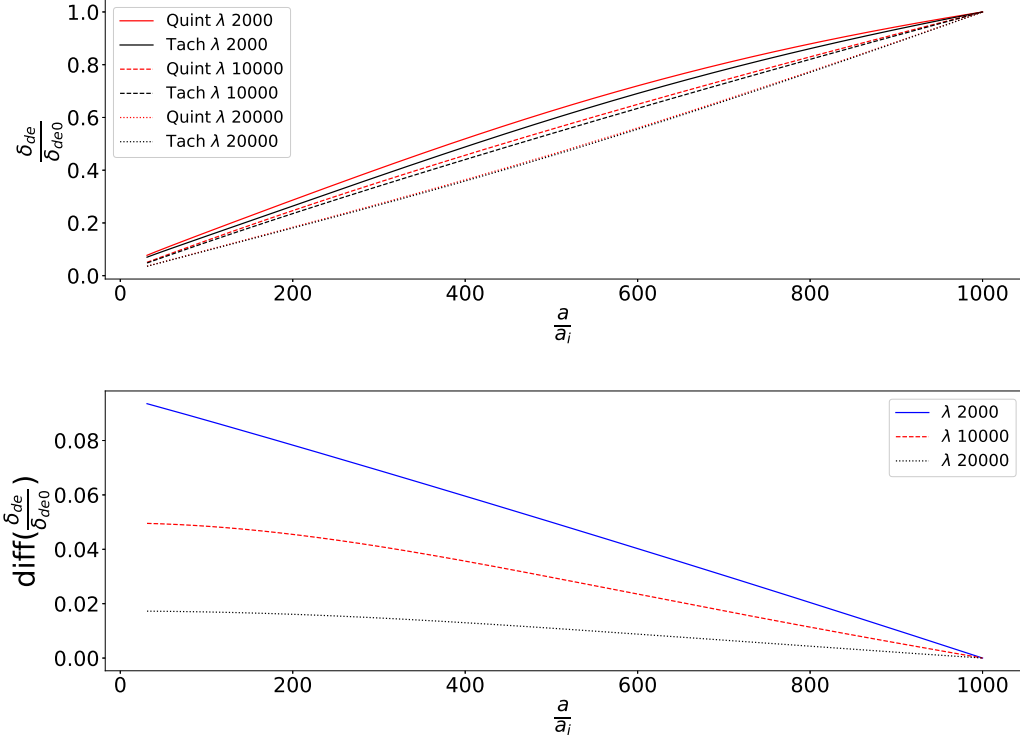


**Figure 6.** Dark energy (DE) density contrast for the CPL case. Curves are neatly clustered here by field type. This suggests that for this particular background evolution, tachyonic field and quintessence field evolve similarly for a particular lengthscale.

These two potentials have some interesting features and have been studied in detail [11, 49]. These potentials have been constrained using low redshift data in [22, 23]. In [22], tachyonic models were constrained using low redshift data from supernova, Hubble parameter measurements, and BAO data. Evolution of perturbations was considered in [23] and redshift space distortion data was used for model comparisons. These models have not yet been constrained using CMB data. We use CLASS with MontePython to constrain the tachyonic models (with the above-mentioned potentials) using Planck 2018 data [50]. We use the following combinations of data:

- CMB (Planck 2018 high-l TT,TE,EE, low-l EE, low-l TT, lensing) [44]
- BAO (Boss Data Release 12 [45, 46], small-z BAO data from 6dF Galaxy Survey [47] and SDSS DR7 main Galaxy sample [48])
- Combination of the above-mentioned CMB and BAO data.
- JLA data [51].

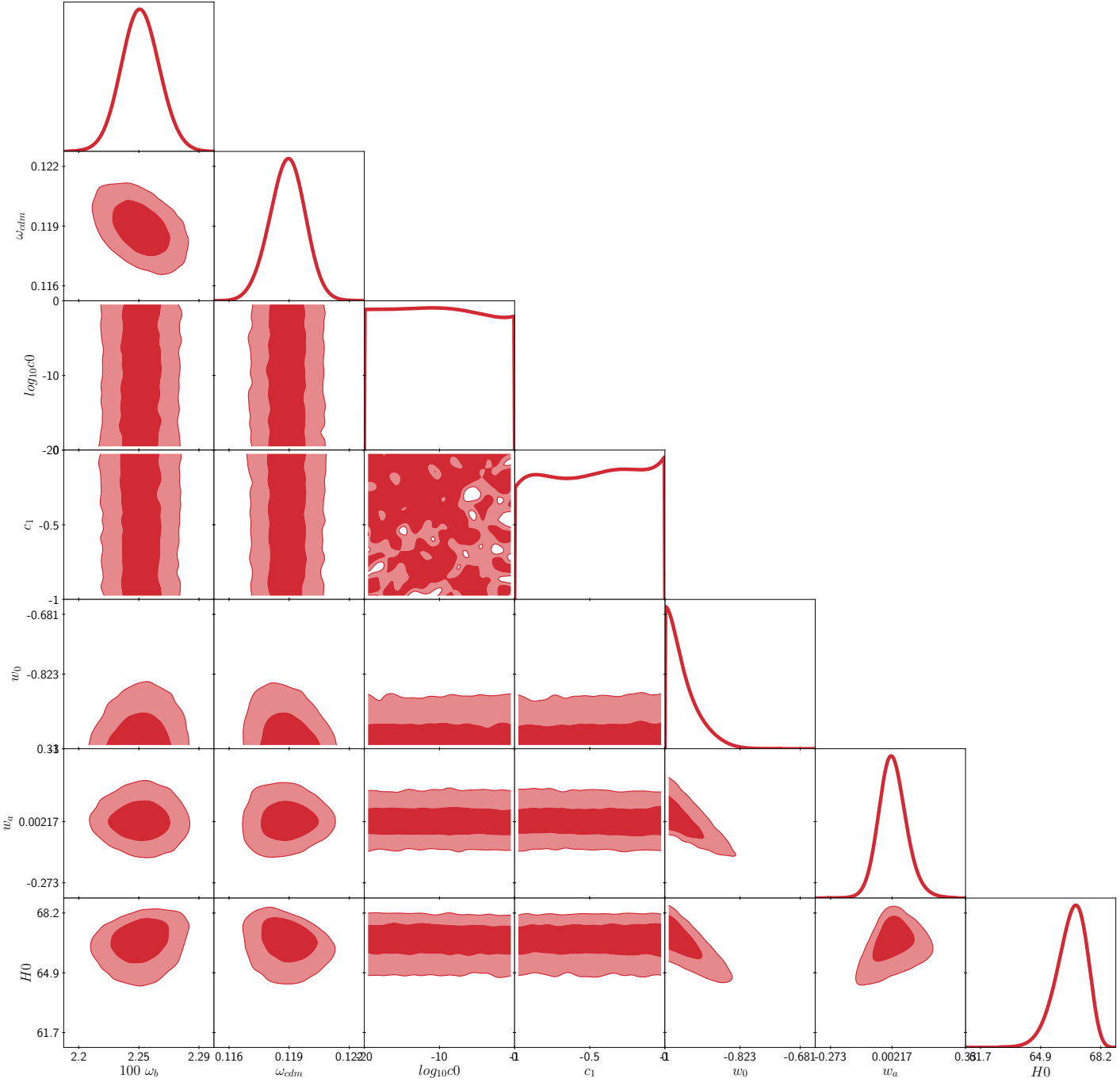


**Figure 7.** Triangle plot: While background cosmological parameters like density parameters,  $H_0$ ,  $w_0$ ,etc. are well constrained, perturbation related parameters like  $c_s^2$  remain unconstrained.

### 6.1. Results

We first consider constraints on parameters that only concern background evolution and are needed irrespective of potentials: density parameter for dark matter and the Hubble constant. In figure 9, we plot contours for present-day matter density contrast

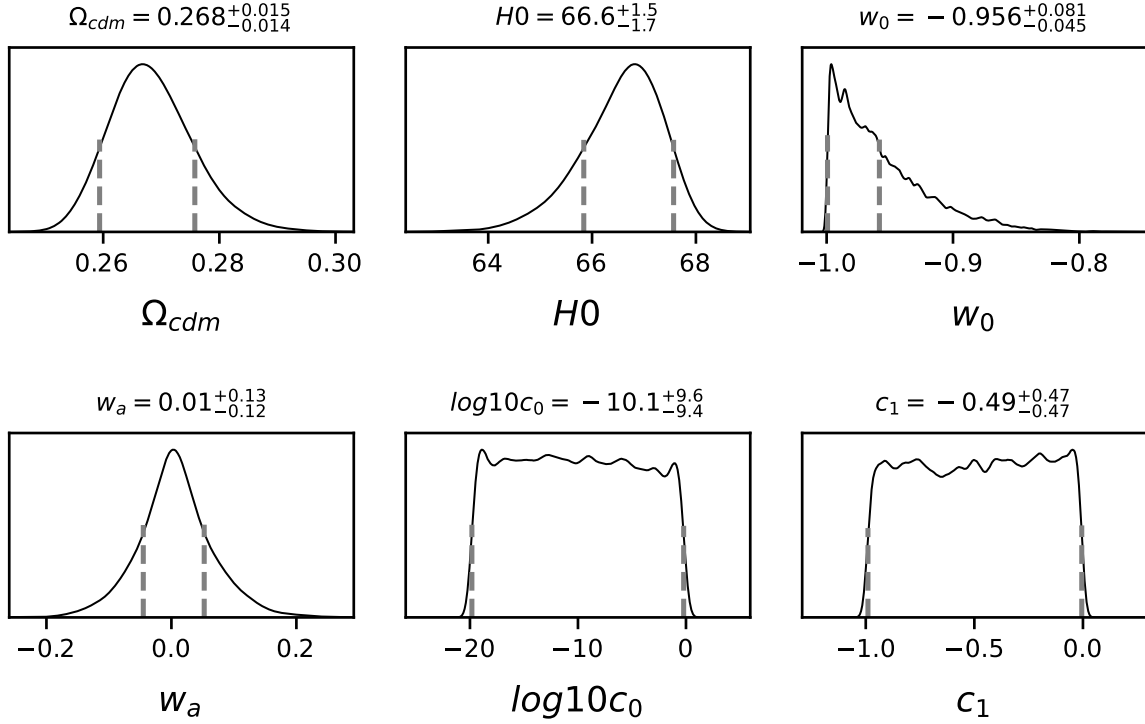


**Figure 8.** 1-dimensional posterior distributions. Vertical dashed lines mark half-maximum x-coordinates while the limits quoted at top are  $2\sigma$  limits.

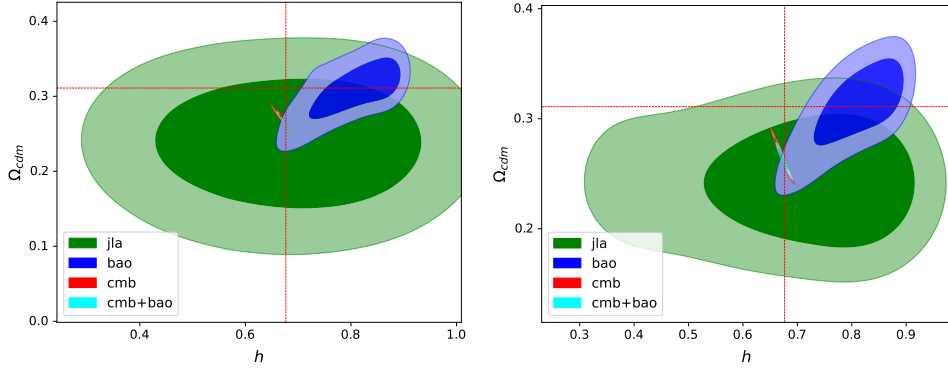


**Figure 9.** 2-d plots for present day matter density parameter  $\Omega_{cdm}$  and Hubble parameter ( $h$ ). Left panel is for exponential potential while right one is for inverse square. Red lines show the best-fit values for  $\Lambda CDM$  model from Planck 2018 [44]. CMB data, as already known, shrinks the constrained region.  $H_0$  tension is not resolved by tachyonic models considered here.

$(\Omega_{cdm})$  and dimensionless Hubble constant ( $h$ ). CMB data provides tight constraints. The best fit values of these parameters, from the  $\Lambda CDM$  model based CMB constraint in Planck 2018 cosmo parameters paper, is represented by red lines in the figure. We find that the best-fit value (2-d) lies in the 1-sigma region of the JLA data, but it is out of 2-sigma regions for CMB and BAO data constraints. While  $h$  is consistent

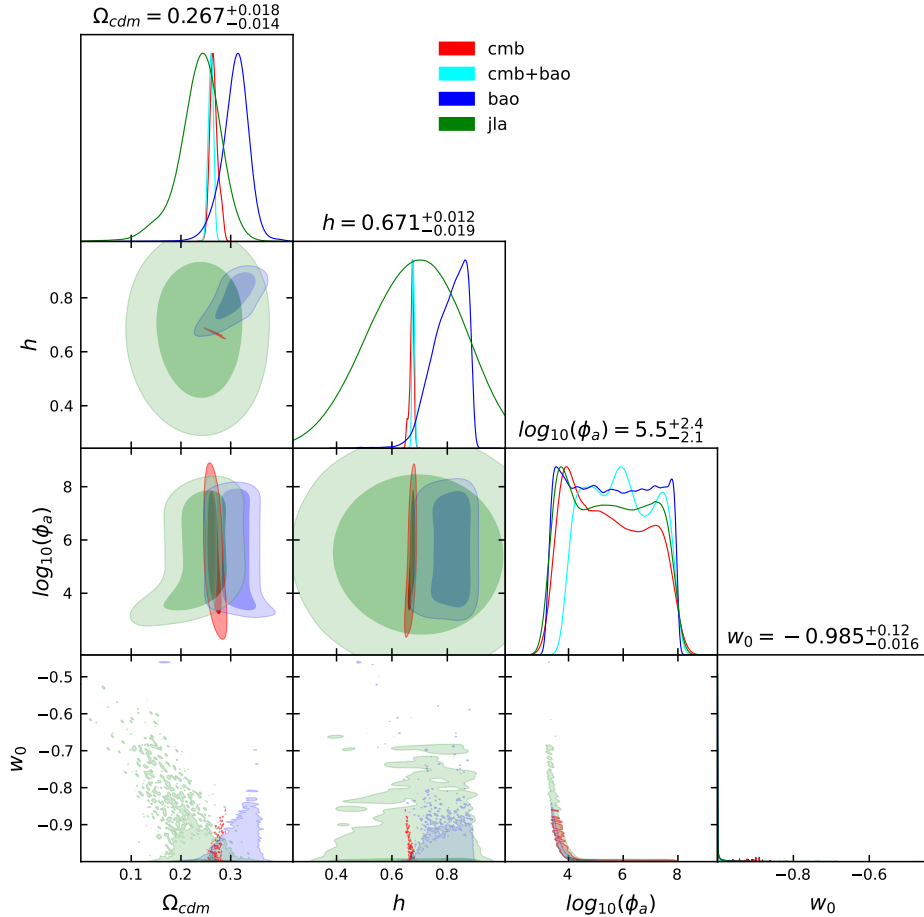


**Figure 10.** Triangle plot using four combinations of data, for exponential potential. Potential parameter  $\phi_a$  is slightly constrained to be greater with certain minima. While  $\phi_a$  appears to have nonlinear correlations with  $w_0$ ,  $w_0$  is constrained be close to  $-1$ .

(within 2-sigma regions), it is  $\Omega_{cdm}$ , which is lower for these tachyonic field based cosmological models. So, inference of dark matter content of the Universe shows dark energy model dependence, when considering extensions beyond  $\Lambda$ . In figure 10, we present the triangle plot for exponential (exp) potential with potential parameter  $\phi_a$  and present-day equation of state  $w_0$ , included along with density and Hubble parameter.  $w_0$  is constrained to be close to  $-1$ . The potential parameter  $\phi_a$  is not constrained by any of the used data. Triangle plot for inverse-square (insq) potential is presented in figure 11. Again, potential parameter  $n$  is allowed a very wide region and  $w_0$  is very close to  $-1$ . Plots with  $\sigma_8$  are shown in figures 12 and 13. The constraints for  $\sigma_8$  for two potentials agree with each other as well as with that for  $\Lambda CDM$ . This is again a manifestation of the fact that the models which have same background evolution and are close to  $\Lambda$  are extremely difficult to distinguish.

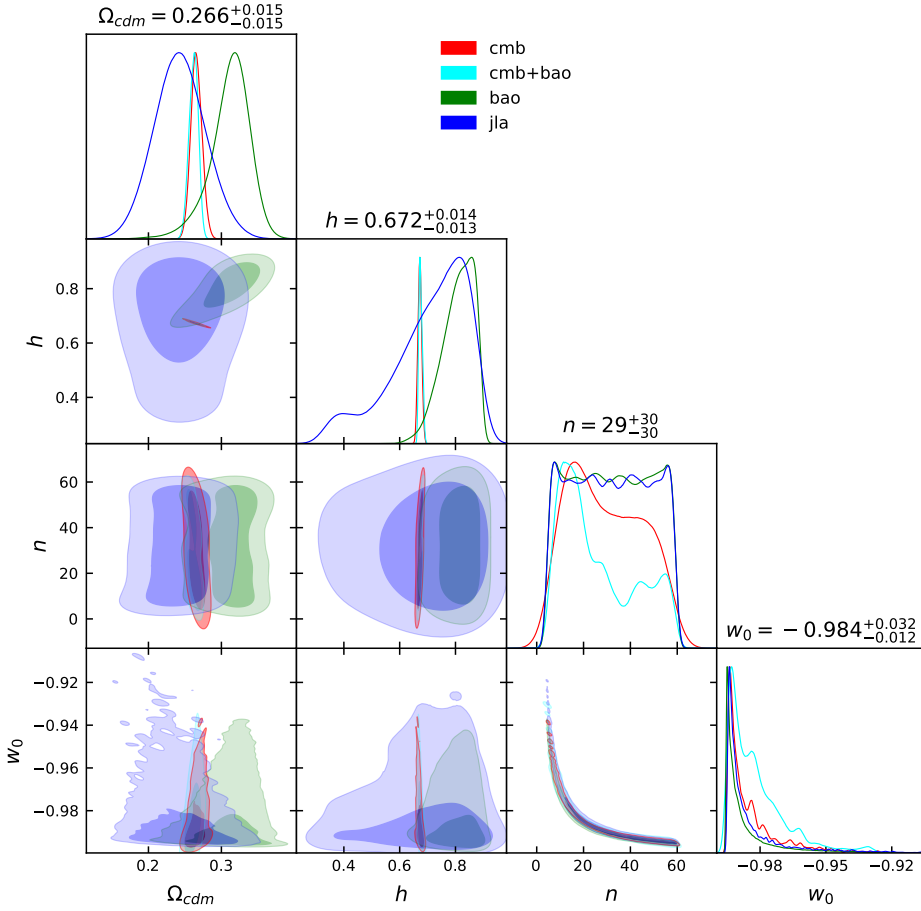


**Figure 11.** Triangle plot using four combinations of data, for inverse square potential. Results are somewhat similar to that for exponential case as potential parameter  $n$  is slightly constrained and is correlated to  $w_0$ . A particular value of  $w_0$  is favoured, which is not  $-1$ , but is close to it.

## 7. Summary & Prospects

We have studied the prospects of using linear perturbation theory to distinguish two different models of dark energy: quintessence and tachyonic field. Specifically, we investigate the differences in dynamics of perturbations for the same background expansion in both models. This helps us separate the effects coming from different background expansions and differences due to perturbations.

We recast linear theory equations in a form that provides insight into how the systems of perturbations differ in two theories. We show that when the equations for both are written in fluid terms, substituting for corresponding field terms, one of the equations has extra terms for quintessence. These first-order terms are multiplied by  $\omega \equiv (1 + w)$ . This implies that if the background expansion is close to  $w = -1$ , differences between the two models diminish.

We calculated and showed the evolution of quantities like  $\psi$  and its derivative, which affects the observables. These numerical calculations demonstrate the theoretical

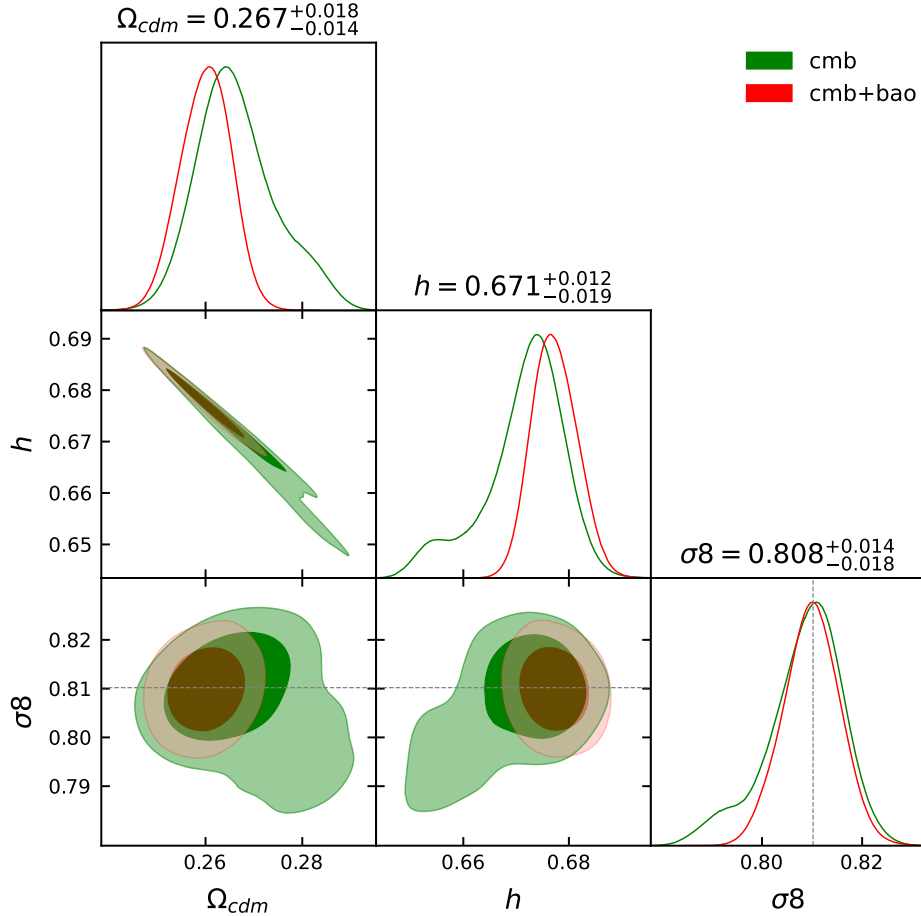


**Figure 12.** Triangle plot with  $\sigma_8$  for the exponential potential. The value of  $\sigma_8$  is compatible with that for  $\Lambda CDM$  from Planck 2018 (plotted as line in this figure).

dependence on the factor of  $(1 + w)$ .

We find that the differences between models while being small at all scales are largest around the scale of 10000 Mpc. We believe that this is due to the difference between the effective speed of sound in two models and that this difference is seen in the transition scales from suppression of perturbations at small scales to growth at large scales.

We used the definition of effective  $c_s^2$  for two models to write a parametric form for  $c_s^2 (\equiv c1 * w + c0)$  which incorporates both fields as instances of particular values of the parameters. We then used CMB data to constrain this parametric form to see if we can distinguish two models and find that two parameters  $c0$  and  $c1$  remain unconstrained.

We modified the CMB anisotropy code CLASS to incorporate tachyon models. We then used it to constrain common tachyonic potentials:  $V \propto \exp(-\frac{\phi}{\phi_a})$  and  $V \propto \phi^{-2}$  using CMB and other data. We find that the parameters are very weakly constrained.

We have shown that it is very difficult to distinguish between these two classes of models at large scales where linear perturbation theory is applicable. We have also shown that this is primarily because only models with  $(1 + w) \ll 1$  are allowed and in

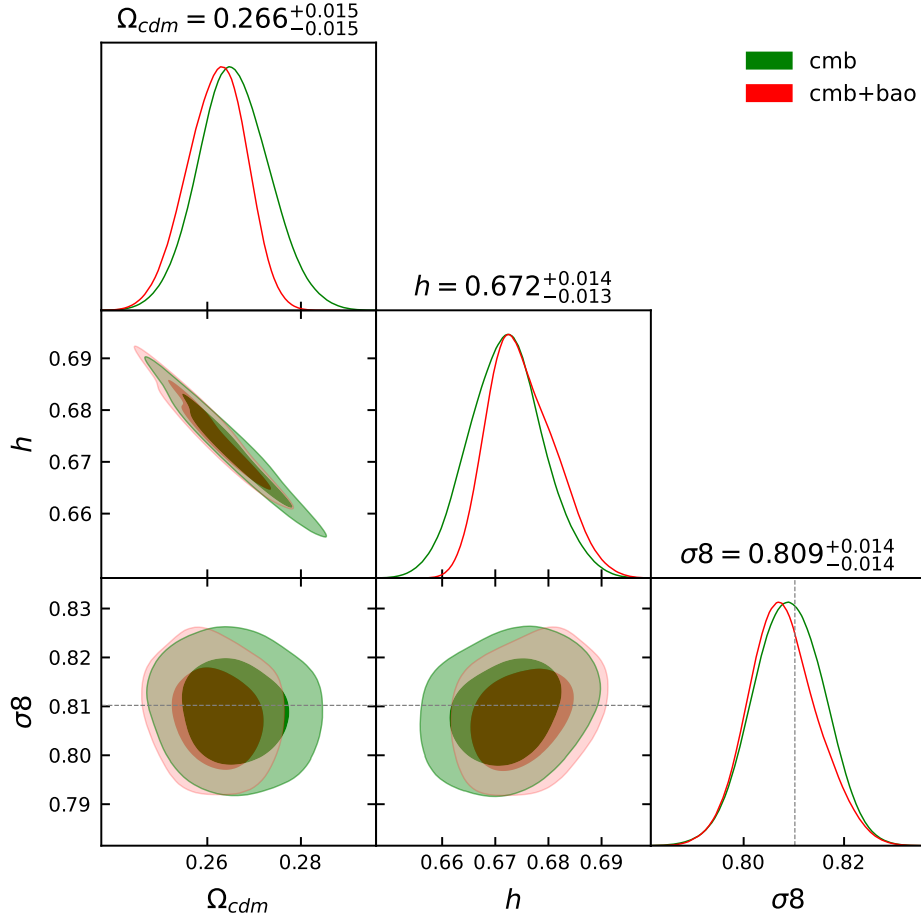


**Figure 13.** Triangle plot with  $\sigma_8$  for the inverse square potential. The constraints are comparable with those for exponential potential as well as  $\Lambda CDM$

this regime, the differences between the two classes of models are effectively of second order. Combined with our earlier work where we have explored these models at small scales using spherical collapse, it appears that there are no obvious observables available at present that may be used to distinguish between these two classes of models if the expansion history is the same. We can conclude that at least for these two classes of dark energy, as also for a fluid model of dark energy, the choice of class of models is irrelevant and calculation of observables may be done in any model. On one hand, this is a potential simplification of calculations, on the other hand, it means that we cannot know which of the models is the true model for dark energy.

We are exploring the following to broaden the scope of our conclusions.

- Working out forecasts to find out the sensitivity of observations required to differentiate between the class of models. This will allow us to see whether future observations can potentially distinguish between the two classes of models. A comparison with the capabilities of upcoming surveys is required to ascertain whether the problem can be solved in the coming years.

- Generalize the analysis to other classes of models to check whether the feature of a prefix of  $(1 + w)$  in model-dependent terms is generic or specific to the classes studied here. We would like to be able to check at least some classes of models with minimal coupling.
- Going beyond linear theory to see if a higher-order calculation or a general numerical relativity calculation at small scales can bring out some features that are not accessible in the two limiting cases we have used so far.

### **Acknowledgment**

All the computational work was done on computing facilities provided by IISER Mohali. This research uses NASA's astrophysics data system (ADS) services.

## Appendix A. Equations in Synchronous Gauge

Here we present the equations required for modification of CLASS for tachyonic field. Since synchronous gauge is the default gauge in CLASS, we write the equations in this gauge. Quintessence with some potentials are already implemented in CLASS, one can simply follow the same structure for incorporating the tachyonic models. Here, we present equations for both quintessence and tachyonic field because this helps on modifications comparing with quintessence implementation.

Note: In this section, we use conformal time and prime represents derivative wrt to conformal time.

Field dynamics equation: For tachyonic models

$$(\delta\phi)'' = \left[1 - \frac{\phi'^2}{a^2}\right] \left[a^2(\delta\phi) \left\{ \frac{(V_{,\phi})^2}{V^2} - \frac{(V_{,\phi\phi})^2}{V^2} \right\} + \nabla^2(\delta\phi) - \frac{\phi'h'}{2}\right] \\ + (\delta\phi)' \left[ -\frac{2a'}{a} + 9\frac{a'}{a} \frac{\phi'^2}{a^2} + 2\frac{V_{,\phi}}{V^2} \phi'^2 \right] \quad (\text{A.1})$$

For quintessence

$$(\delta\phi)'' = -a^2(\delta\phi)(V_{,\phi\phi}) - \frac{\phi'h'}{2} - \frac{2a'}{a}(\delta\phi)' + \nabla^2(\delta\phi) \quad (\text{A.2})$$

Density ( $\delta\rho$ ) and pressure perturbations ( $\delta p$ ): For tachyonic field

$$(\delta\rho) = \frac{(\delta\phi)(V_{,\phi})}{\sqrt{1 - \frac{\phi'^2}{a^2}}} + \frac{V\phi'(\delta\phi)'}{a^2 \left[1 - \frac{\phi'^2}{a^2}\right]^{3/2}} \quad (\text{A.3})$$

$$(\delta p) = -(\delta\phi)(V_{,\phi}) \sqrt{1 - \frac{\phi'^2}{a^2}} + \frac{V\phi'(\delta\phi)'}{a^2 \sqrt{1 - \frac{\phi'^2}{a^2}}} \quad (\text{A.4})$$

For quintessence

$$(\delta\rho) = (\delta\phi)(V_{,\phi}) + \frac{\phi'(\delta\phi)'}{a^2} \quad (\text{A.5})$$

$$(\delta p) = -(\delta\phi)(V_{,\phi}) + \frac{\phi'(\delta\phi)'}{a^2} \quad (\text{A.6})$$

Effective velocity perturbations:

For tachyonic field

$$(\bar{\rho} + \bar{p})\theta = ik^j(\delta T)_j^0 = \frac{\phi'}{a^2} k^2(\delta\phi) \frac{V}{\sqrt{1 - \frac{\phi'^2}{a^2}}} \quad (\text{A.7})$$

For quintessence

$$(\bar{\rho} + \bar{p})\theta = \frac{\phi'}{a^2} k^2(\delta\phi) \quad (\text{A.8})$$

## References

- [1] A. G. Riess, A. V. Filippenko, P. Challis, A. Clocchiatti, A. Diercks, P. M. Garnavich, R. L. Gilliland, C. J. Hogan, S. Jha, R. P. Kirshner, B. Leibundgut, M. M. Phillips, D. Reiss, B. P. Schmidt, R. A. Schommer, R. C. Smith, J. Spyromilio, C. Stubbs, N. B. Suntzeff, and J. Tonry, “Observational evidence from supernovae for an accelerating universe and a cosmological constant,” *The Astronomical Journal*, vol. 116, pp. 1009–1038, sep 1998.
- [2] S. Perlmutter, G. Aldering, G. Goldhaber, R. A. Knop, P. Nugent, P. G. Castro, S. Deustua, S. Fabbro, A. Goobar, D. E. Groom, I. M. Hook, A. G. Kim, M. Y. Kim, J. C. Lee, N. J. Nunes, R. Pain, C. R. Pennypacker, R. Quimby, C. Lidman, R. S. Ellis, M. Irwin, R. G. McMahon, P. Ruiz-Lapuente, N. Walton, B. Schaefer, B. J. Boyle, A. V. Filippenko, T. Matheson, A. S. Fruchter, N. Panagia, H. J. M. Newberg, W. J. Couch, and T. S. C. Project, “Measurements of  $\Omega$  and  $\Lambda$  from 42 High-Redshift Supernovae,” *ApJ*, vol. 517, pp. 565–586, June 1999.
- [3] B. P. Schmidt, N. B. Suntzeff, M. M. Phillips, R. A. Schommer, A. Clocchiatti, R. P. Kirshner, P. Garnavich, P. Challis, B. Leibundgut, J. Spyromilio, A. G. Riess, A. V. Filippenko, M. Hamuy, R. C. Smith, C. Hogan, C. Stubbs, A. Diercks, D. Reiss, R. Gilliland, J. Tonry, J. Maza, A. Dressler, J. Walsh, and R. Ciardullo, “The High-Z Supernova Search: Measuring Cosmic Deceleration and Global Curvature of the Universe Using Type IA Supernovae,” *ApJ*, vol. 507, pp. 46–63, Nov. 1998.
- [4] L. Amendola and S. Tsujikawa, *Dark Energy: Theory and Observations*. Cambridge University Press, 2010.
- [5] E. J. Copeland, M. Sami, and S. Tsujikawa, “Dynamics of Dark Energy,” *International Journal of Modern Physics D*, vol. 15, pp. 1753–1935, Jan. 2006.
- [6] A. Joyce, L. Lombriser, and F. Schmidt, “Dark Energy Versus Modified Gravity,” *Annual Review of Nuclear and Particle Science*, vol. 66, pp. 95–122, Oct. 2016.
- [7] R. Caldwell, R. Dave, and P. J. Steinhardt, “Cosmological imprint of an energy component with general equation of state,” *Phys. Rev. Lett.*, vol. 80, pp. 1582–1585, 1998.
- [8] B. Ratra and P. Peebles, “Cosmological Consequences of a Rolling Homogeneous Scalar Field,” *Phys. Rev. D*, vol. 37, p. 3406, 1988.
- [9] R. Caldwell and E. V. Linder, “The Limits of quintessence,” *Phys. Rev. Lett.*, vol. 95, p. 141301, 2005.
- [10] S. Tsujikawa, “Quintessence: A Review,” *Class. Quant. Grav.*, vol. 30, p. 214003, 2013.
- [11] T. Padmanabhan, “Accelerated expansion of the universe driven by tachyonic matter,” *Phys. Rev. D*, vol. 66, p. 021301, 2002.
- [12] J. Bagla, H. K. Jassal, and T. Padmanabhan, “Cosmology with tachyon field as dark energy,” *Phys. Rev. D*, vol. 67, p. 063504, 2003.
- [13] H. Kodama and M. Sasaki, “Cosmological Perturbation Theory,” *Progress of Theoretical Physics Supplement*, vol. 78, pp. 1–166, 01 1984.
- [14] V. Mukhanov, H. Feldman, and R. Brandenberger, “Theory of cosmological perturbations,” *Physics Reports*, vol. 215, no. 5, pp. 203 – 333, 1992.
- [15] C.-P. Ma and E. Bertschinger, “Cosmological perturbation theory in the synchronous and conformal Newtonian gauges,” *Astrophys. J.*, vol. 455, pp. 7–25, 1995.
- [16] W. Hu and S. Dodelson, “Cosmic microwave background anisotropies,” *Annual Review of Astronomy and Astrophysics*, vol. 40, no. 1, pp. 171–216, 2002.
- [17] S. Unnikrishnan, H. K. Jassal, and T. R. Seshadri, “Scalar field dark energy perturbations and their scale dependence,” *Phys. Rev. D*, vol. 78, p. 123504, Dec 2008.
- [18] H. K. Jassal, “Evolution of perturbations in distinct classes of canonical scalar field models of dark energy,” *Phys. Rev. D*, vol. 81, p. 083513, Apr 2010.
- [19] H. K. Jassal, “Comparison of perturbations in fluid and scalar field models of dark energy,” *Phys. Rev. D*, vol. 79, p. 127301, June 2009.
- [20] H. K. Jassal, “Scalar field dark energy perturbations and the integrated Sachs-Wolfe effect,”

Phys. Rev. D, vol. 86, p. 043528, Aug. 2012.

[21] J.-c. Hwang and H. Noh, “Quintessential perturbations during scaling regime,” *Phys. Rev. D*, vol. 64, p. 103509, Oct 2001.

[22] A. Singh, A. Sangwan, and H. Jassal, “Low redshift observational constraints on tachyon models of dark energy,” *Journal of Cosmology and Astroparticle Physics*, vol. 2019, pp. 047–047, apr 2019.

[23] A. Singh, H. Jassal, and M. Sharma, “Perturbations in tachyon dark energy and their effect on matter clustering,” *Journal of Cosmology and Astroparticle Physics*, vol. 2020, p. 008–008, May 2020.

[24] A. Mehrabi, S. Basilakos, and F. Pace, “How clustering dark energy affects matter perturbations,” *MNRAS*, vol. 452, pp. 2930–2939, Sept. 2015.

[25] R. Bean and O. Dore, “Probing dark energy perturbations: The Dark energy equation of state and speed of sound as measured by WMAP,” *Phys. Rev. D*, vol. 69, p. 083503, 2004.

[26] R. de Putter, D. Huterer, and E. V. Linder, “Measuring the speed of dark: Detecting dark energy perturbations,” *Phys. Rev. D*, vol. 81, p. 103513, May 2010.

[27] J. Weller and A. M. Lewis, “Large-scale cosmic microwave background anisotropies and dark energy,” *MNRAS*, vol. 346, pp. 987–993, Dec. 2003.

[28] R. Batista and F. Pace, “Structure formation in inhomogeneous Early Dark Energy models,” *JCAP*, vol. 06, p. 044, 2013.

[29] J. K. Erickson, R. Caldwell, P. J. Steinhardt, C. Armendariz-Picon, and V. F. Mukhanov, “Measuring the speed of sound of quintessence,” *Phys. Rev. Lett.*, vol. 88, p. 121301, 2002.

[30] S. DeDeo, R. R. Caldwell, and P. J. Steinhardt, “Effects of the sound speed of quintessence on the microwave background and large scale structure,” *Phys. Rev. D*, vol. 67, p. 103509, May 2003.

[31] R. K. Sachs and A. M. Wolfe, “Perturbations of a Cosmological Model and Angular Variations of the Microwave Background,” *ApJ*, vol. 147, p. 73, Jan. 1967.

[32] M. Chevallier and D. Polarski, “Accelerating Universes with Scaling Dark Matter,” *International Journal of Modern Physics D*, vol. 10, pp. 213–223, Jan. 2001.

[33] E. V. Linder, “Exploring the Expansion History of the Universe,” *Phys. Rev. Lett.*, vol. 90, p. 091301, Mar. 2003.

[34] M. Pratap Rajvanshi and J. S. Bagla, “Nonlinear spherical perturbations in quintessence models of dark energy,” *J. Cosmology Astropart. Phys.*, vol. 2018, p. 018, June 2018.

[35] M. P. Rajvanshi and J. Bagla, “Erratum: Nonlinear spherical perturbations in quintessence models of dark energy,” *Journal of Cosmology and Astroparticle Physics*, vol. 2020, pp. E01–E01, mar 2020.

[36] Planck Collaboration and e. a. Ade, “Planck 2015 results. XIII. Cosmological parameters,” *A&A*, vol. 594, p. A13, Sept. 2016.

[37] A. Tripathi, A. Sangwan, and H. K. Jassal, “Dark energy equation of state parameter and its evolution at low redshift,” *J. Cosmology Astropart. Phys.*, vol. 2017, p. 012, June 2017.

[38] A. Lewis, A. Challinor, and A. Lasenby, “Efficient Computation of Cosmic Microwave Background Anisotropies in Closed Friedmann-Robertson-Walker Models,” *ApJ*, vol. 538, pp. 473–476, Aug. 2000.

[39] J. Lesgourgues, “The Cosmic Linear Anisotropy Solving System (CLASS) I: Overview,” *arXiv e-prints*, p. arXiv:1104.2932, Apr. 2011.

[40] D. Blas, J. Lesgourgues, and T. Tram, “The Cosmic Linear Anisotropy Solving System (CLASS). Part II: Approximation schemes,” *J. Cosmology Astropart. Phys.*, vol. 2011, p. 034, July 2011.

[41] J. Lesgourgues, “The Cosmic Linear Anisotropy Solving System (CLASS) III: Comparison with CAMB for LambdaCDM,” *arXiv e-prints*, p. arXiv:1104.2934, Apr. 2011.

[42] B. Audren, J. Lesgourgues, K. Benabed, and S. Prunet, “Conservative Constraints on Early Cosmology: an illustration of the Monte Python cosmological parameter inference code,” *JCAP*, vol. 1302, p. 001, 2013.

[43] T. Brinckmann and J. Lesgourgues, “MontePython 3: boosted MCMC sampler and other

features,” 2018.

- [44] Planck Collaboration and A. et. al, “Planck 2018 results. VI. Cosmological parameters,” A&A, vol. 641, p. A6, Sept. 2020.
- [45] A. et. al MNRAS, vol. 470, pp. 2617–2652, Sept. 2017.
- [46] M. A. Buen-Abad, M. Schmaltz, J. Lesgourgues, and T. Brinckmann, “Interacting dark sector and precision cosmology,” J. Cosmology Astropart. Phys., vol. 2018, p. 008, Jan. 2018.
- [47] F. Beutler, C. Blake, M. Colless, D. H. Jones, L. Staveley-Smith, L. Campbell, Q. Parker, W. Saunders, and F. Watson, “The 6dF Galaxy Survey: baryon acoustic oscillations and the local Hubble constant,” MNRAS, vol. 416, pp. 3017–3032, Oct. 2011.
- [48] A. J. Ross, L. Samushia, C. Howlett, W. J. Percival, A. Burden, and M. Manera, “The clustering of the SDSS DR7 main Galaxy sample - I. A 4 per cent distance measure at  $z = 0.15$ ,” MNRAS, vol. 449, pp. 835–847, May 2015.
- [49] A. Sen, “Rolling tachyon,” *Journal of High Energy Physics*, vol. 2002, pp. 048–048, apr 2002.
- [50] Planck Collaboration and e. a. Aghanim, “Planck 2018 results. I. Overview and the cosmological legacy of Planck,” A&A, vol. 641, p. A1, Sept. 2020.
- [51] B. et. al, “Improved cosmological constraints from a joint analysis of the SDSS-II and SNLS supernova samples,” A&A, vol. 568, p. A22, Aug. 2014.